FIRST RESULTS FOR THE ROSACE AUTONOMOUS ORBIT DETERMINATION SYSTEM USING DEVIATION ON CCD

Isabelle ESCANE
Nicolas DELONG
Franz NEWLAND

Centre National d'Etudes Spatiales
18, avenue Edouard Belin
31401 Toulouse Cedex 4, France
Isabelle.Escane@cnes.fr
Nicolas.Delong@cnes.fr
franz@kaula.cst.cnes.fr

ABSTRACT *– The ROSACE station is a low cost ground system for orbit determination of geosynchronous or low angular speed spacecraft, using a Newtonian telescope and a CCD detector in its focal plane, which can achieve an angular measurement accuracy of 1 arc second (3 σ). The paper is organized into three parts: the ROSACE concept is detailed, the image analysis algorithms are described and the first results obtained for geostationary satellites using the ROSACE prototype station installed at the Observatory of Haute Provence are presented.*

KEYWORDS: CCD, image processing, orbit determination, star catalogue, satellite ground station.

INTRODUCTION

The ROSACE station is a low cost ground system for orbit determination of geosynchronous spacecraft or low angular speed spacecraft using a Newtonian telescope and a CCD detector in its focal plane. The ROSACE station concept has been described in earlier publications during its conception (in particular [1] and [2]). This paper provides the proof of concept by presenting the final design as implemented in the first operational ROSACE station, and it further provides the first results for the station. The fundamental principle of the ROSACE station is to generate a measurement of the angular separation of satellites relative to their background star field. This avoids traditional tropospheric errors as, though the absolute image error from refraction or other disturbance may be great, the difference in the effect of the error between two points in the field of view is much smaller, and all measurements of satellite position are made relative to the stars within this field of view. The precision in measurement of the absolute satellite position is then achieved courtesy of star catalogues, which provide precise and accurate absolute star positions.

To allow even dim satellites to be detected, the telescope follows the satellite whilst taking the image in order that the light from it falls on the same CCD array pixels throughout the shot. As a result, the stars are seen to travel across the field of view during the shot (in parallel straight lines when tracking

geostationary satellites). The mid-point of each star path and the centre of the satellite pixels are then used to determine the angular separation η and the phase φ between the direction of the star path and the star-satellite axis, as shown in Figure 1.

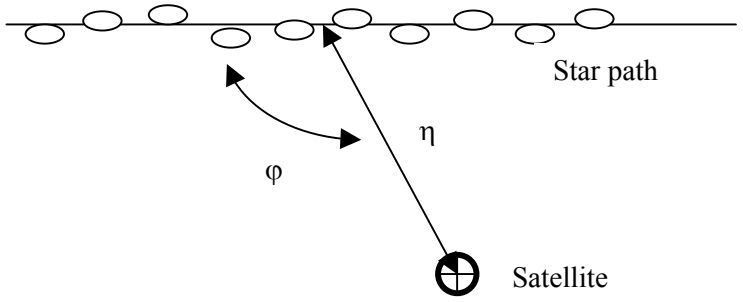

Figure 1 The basic ROSACE measurements.

The position of each star track centre is calculated in an equatorial inertial frame of reference using the TYCHO star catalogue, from which the angular position of the satellite is deduced. For each satellite-star pair, the classical position measurements of satellite azimuth and elevation relative to the ROSACE station are then calculated. The station is intended to provide measurements to a precision of one arc-second for geostationary satellites.

The possible applications of ROSACE are diverse:

- For calibrating orbitographic antennas, as the ROSACE measurements are more accurate than most positioning systems for stationkeeping activities.
- To provide redundancy or to complement classical position measurements, with the benefit that the station does not interfere with or affect operational procedures (unlike active tracking methods which require scheduling etc.).
- For surveillance of satellites or debris near the geostationary arc, as ROSACE is a passive observation system that requires no equipment on board the observed objects. This also allows satellites to be tracked in cases where their tracking transponders or other systems have failed, for example.
- For observing satellites in collocation, for which ROSACE is able to generate an independent measure of the relative separation and phase of the collocated satellites, for determining their relative orbit(s).

A description of the ROSACE station design follows, followed by details of the image processing and position determination algorithms. Finally, the first results obtained from the prototype ROSACE station installed in 2001 at the Observatory of Haute Provence (OHP) are presented. These consist of the first geostationary satellite orbit restitutions performed with the station.

DESCRIPTION OF THE ROSACE STATION DESIGN

The hardware

The aim of ROSACE is to provide a precise satellite localisation system at low cost relative to other systems of equivalent precision (e.g. turnaround systems), both in terms of construction and installation *and* operation and maintenance. Its design consists of a Newton telescope equipped with a CCD camera, housed under a cupola and driven entirely by a workstation. A remote management centre communicates with the station only to provide it with the observation planning at the start of the evening and to

recuperate the satellite position data the following morning. During the night, the station functions completely autonomously.

In sizing the station, a compromise has to be drawn between the optical performance desired and the cost of the hardware and supporting software. The technical objective defined for ROSACE was therefore to observe objects of up to magnitude 19 (for example, a Telecom satellite magnitude is about 9.5) and stars of up to magnitude 10.5. For the prototype station, a Newton telescope of 500mm diameter and a focal length of 1900mm was accordingly selected. An equatorial mount is not necessary for orienting the telescope due to the nature of the satellite orbits to be followed, hence the station design makes use of an azimuthal mount. Each axis of the mount is equipped with a stepped motor and angular coding and command electronics to point the telescope in the desired direction. The resulting pointing precision is 20".

The detector at the centre of the telescope is a CCD camera of 1024*1536 pixels. The field of view provided by the telescope and covered by the CCD array is approximately 0.3*0.4 degrees, each pixel thus covering approximately 1", or 170m in the geostationary arc. An analogue to digital converter captures the analogue signal from each element of the CCD array and stores it ready for acquisition by the station PC, which uses QMIPS software [3] for handling the image collection, storage and subsequent transmission to the station's workstation. The detection block also contains a high-pass image filter, the controls for focussing the telescope, the shutter and a device for rotating the CCD array's field of view to maintain the star tracks approximately parallel to the long edge of the array.

A UNIX workstation controls the operation of the ROSACE station. It is supplied with planning files for an observation campaign from a central control centre via a remote link, and then executes autonomously during the measurement campaign. Its software and function is described in more detail in the next section.

The cupola that protects the station hardware is 3.5m in diameter. Its rotation is coupled to the azimuthal movement of the telescope. The slot opening in the cupola dome is opened automatically by the station electronics at the start of each observation campaign. The telescope under its cupola is shown in Figure 2.

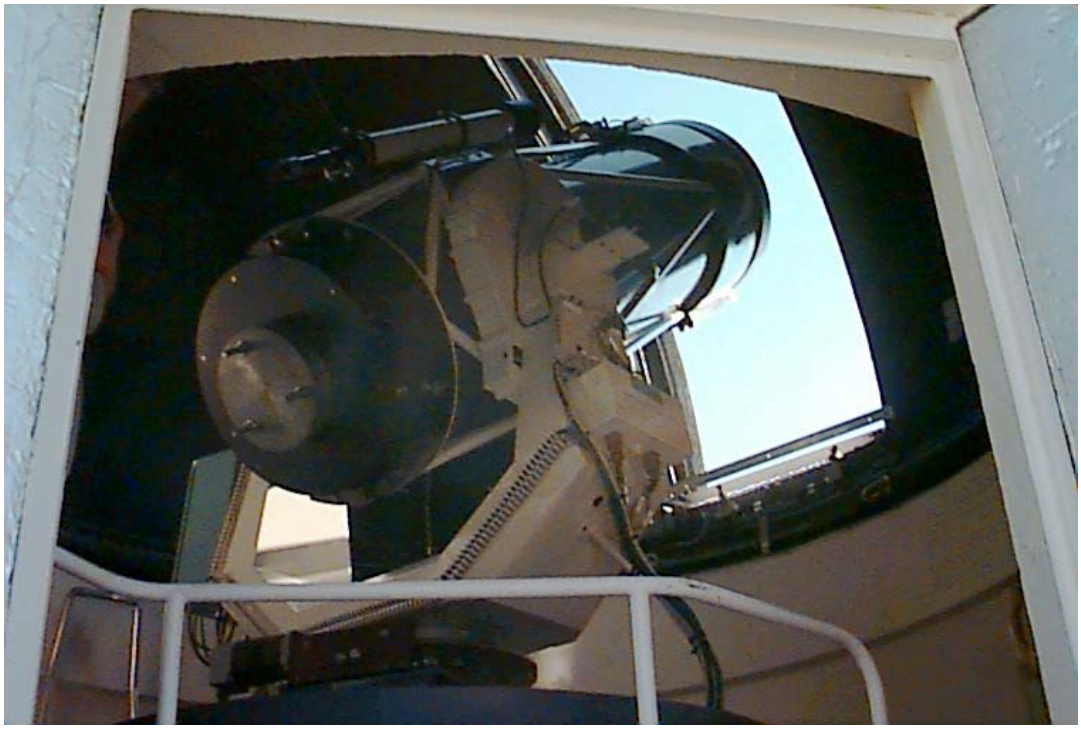

Figure 2 The ROSACE station telescope in its cupola

The ROSACE station has its own weather station which is installed on a post near the cupola. The meteorological instruments consist of an anemometer, barometer, hygrometer and a thermometer. These provide wind and rain measurements necessary for securing the station in adverse conditions (any campaign in progress is stopped, only as long as necessary, in the case of unfavourable weather), and also provide pressure, temperature and humidity data that are used in calculating atmospheric refraction effects on the CCD images collected. The station's GPS receiver provides the time reference, and allows the image capture to be timestamped precisely.

A central control centre connected to the station via a wide area network is used to perform the campaign planning (specification of the satellites to track, etc.) and collect the resulting orbit measurements. After creating the planning files and transferring them to the ROSACE station, the control centre remotely sends a request to the station's workstation to start the campaign. At the end of the night, it collects the position measurements from the station.

The software

There are three main modules of software used by the station's workstation in carrying out its measurement campaign:

The **supervisor module** controls the station hardware. It orders changes in orientation of the telescope for the next image desired, as requested by the image selection module, and commands rotations of the field of view and changes in the position of the CCD in the focal plane. During image collection, it commands the shutter and triggers the QMIPS image acquisition on the station PC. The image is transferred to the workstation by QMIPS, and is analysed by the image processing module, which in turn provides its results (success or failure of generation of a measurement) to the supervisor and image selection modules.

At the same time as receiving the images, the supervisor module also regularly receives:

- Weather data from the meteorological instruments: in case of rain or strong wind, the supervisor commands the closure of the cupola slit, and on improvement of conditions, commands its reopening.
- Time and date information from the GPS receiver that updates the workstation date and time. Precise timestamps for the shutter opening and closing times are necessary to provide precise measurements.

The **image selection module** selects the next position to view and the parameters for the next image, in real time. To select the next position to view, it uses the planning performed before starting the campaign for each of the orbital positions to be observed during the night and the results of the image processing already performed during the campaign (satellites for which few measures have been able to be generated thus far are returned to by preference), as well as the weighting given to each position (predefined in the campaign planning). The image recording parameters (telescope rotation during recording, time to start image acquisition, number and length of shutter cycles during the image acquisition) are then read from the planning files by the image selection module.

The **image processing module** performs the image analysis and returns the satellite position measures or reasons for failure to generate a measure, and is described in more detail later in this paper.

In addition, support software is used to generate the planning files needed during the campaign. The planning phase is performed prior to starting a campaign, typically in the control centre, and consists of defining each orbital position to be observed, and generating all possible image collection opportunities at each position taking into account star location, lunar masking and desired interval between measurements. The operator is only required to enter the approximate orbital parameters for the satellites of interest (to allow the field of view to be oriented correctly and to provide the information to allow the telescope to follow the satellite approximately during each image collection). The resulting planning files contain the characteristics of the images to be captured, optimised to contain as many complete star tracks as possible. The software is equally able to handle the case of orbital positions which encompass multiple satellites in collocation, in which case the image planning also optimises to include all of the collocated satellites where possible and appropriate.

The choice of site

The main constraint on quality and availability of ground-based optical satellite orbit measurements is the state of the sky, as observations are clearly only possible on cloud-free nights. The choice of site for a ROSACE station is therefore a key component to its performance: it is necessary to use a site offering the maximum number of clear nights per year. It is however possible to improve system availability by using multiple ROSACE stations sufficiently far apart to avoid being affected by the same weather conditions. In addition to weather constraints, observing the satellites of interest as high as possible in the sky minimises refraction effects, which despite having a reduced impact due to the approach described, still increase with distance from the subsatellite point.

For the first ROSACE prototype a suitable site in France was sought, to ease any necessary intervention required at the station itself whilst proving the concept, despite the fact that overseas sites would have offered significantly more nights suitable for ROSACE-type observations. The site selected was the Observatory of Haute Provence (OHP) in south-east France, both because of its high preponderance of clear nights for a French site, and because it offered extensive existing infrastructure to help with both installation and maintenance of the site. The first ROSACE station was installed at OHP at the beginning of 2001.

Due in part to technical difficulties (which have now been resolved) and partly to poor weather conditions this year, it has not been possible to run as many measurement campaigns to date as had been hoped. The initial results presented here are promising, however, and improvements currently under investigation, in particular with regard to the image processing, are hoped to offer greater availability of measurements under less-than-ideal optical conditions in future.

IMAGE PROCESSING

The aim of the image processing module is to provide the position of the satellite or satellites in azimuth and elevation from the station. To achieve this, the module makes use of the following information:

- The image collected, i.e. the quantised CCD array values
- The mount position during the image acquisition
- Satellite and star catalogues
- The meteorological conditions
- The characteristics and tolerances of the hardware used in the station

Before identifying the objects of interest in the image, the image is treated in order to improve its subsequent interpretation. In effect, the atmosphere, the telescope, the CCD and its electronics all alter the image to some extent, and the initial filtering aims to reduce these effects.

The complete chain of image processing is as follows:

- Image thresholding
- Radiometric correction of the image
- Image filtering, to improve the signal to noise ratio of the data
- Extraction of the satellite and star pixel clusters in the image
- Detection of aligned pixel clusters which are likely to represent moving objects (i.e. detection of the star tracks)
- Identification of the objects found (cross-referencing with the star and satellite catalogues)
- Calculation of the azimuth and elevation of the fixed objects found (i.e. the satellites)

The CCD array image

The images acquired by the CCD camera are collected as 1024*1536 pixel matrices. The pixels values are 15-bit quantised values of the analogue output of the CCD array elements, which themselves are a measure of the photometry of the region captured in the image. Post-collection, the images are currently reduced using a 2*2 pixel binning (summing of CCD array elements in squares of 2*2 elements), resulting in an image of 512*768 pixels, 700Koctets. This is a temporary processing step both for keeping the image size down for storage and transfer reasons, and to enable faster image processing, during the station validation and verification phase. It is intended to move to the full resolution in the near future. Figure 3 shows an example CCD image for two collocated satellites.

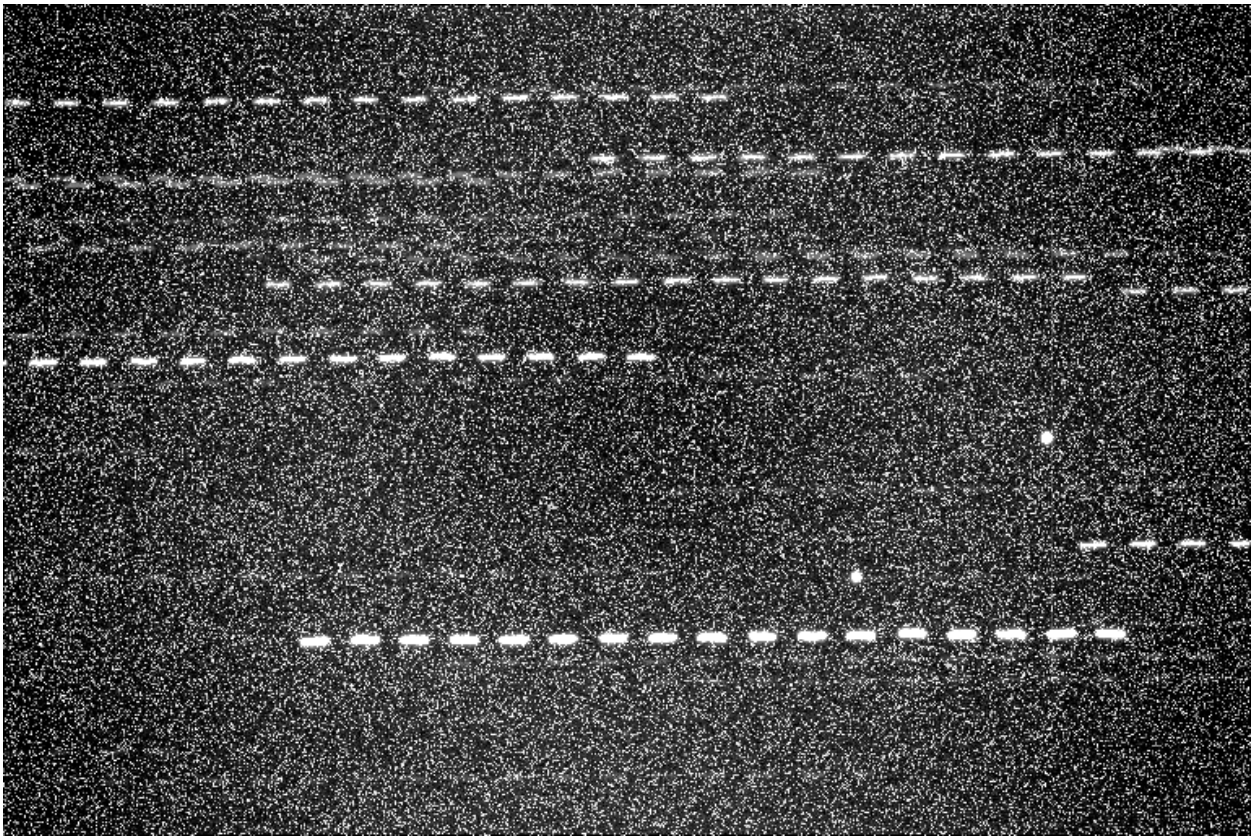

Figure 3 A ROSACE image from 20:20UTC, 1st February 2001, depicting Telecom 2A and 2D and a number of star tracks

Thresholding

The thresholding operation consists of determining the photometry threshold value above which the pixels are considered to be illuminated (either by the satellite(s) of interest or the stars in the field of view). This threshold is used both for the radiometric correction, which performs a calculation on the pixels considered as depicting deep space (i.e. below the threshold), and subsequently for the cluster extraction phase, which extracts connected pixels above the threshold.

The histogram of image pixels as a function of their photometry shows that the majority of image pixels have a photometry centred around a median value. The majority of image pixels also depict deep space, with those depicting star and satellite clusters having typically higher photometric values (e.g. Figure 5). The assumption is made that the histogram of the deep space pixels is symmetric.

The threshold of star and satellite cluster pixels is therefore determined using a method of symmetrication of the image histogram (see also [4] for further justification of this approach). This method makes use both of a simple and a cumulative histogram for a cross-section of the image, as shown in Figure 4.

The mean photometry value of the deep space region is determined as the axis of symmetry of the simple histogram. The spread of the deep-space region of the histogram is determined using the cumulative histogram and the coefficient of confidence, which is a measure of likelihood that any given image pixel depicts deep space (i.e. it is a measure of the number of illuminated pixels expected in an image). A lower photometric threshold is calculated from the coefficient of confidence. This is the smallest value for which the percentage of pixels in the cumulative histogram is above the coefficient of confidence. The spread of deep space photometric values is then taken as twice the difference between the mean deep space photometry and the lower threshold. The corresponding upper threshold of interest, or threshold of lit pixels, results from the symmetry about the mean deep space photometric value.

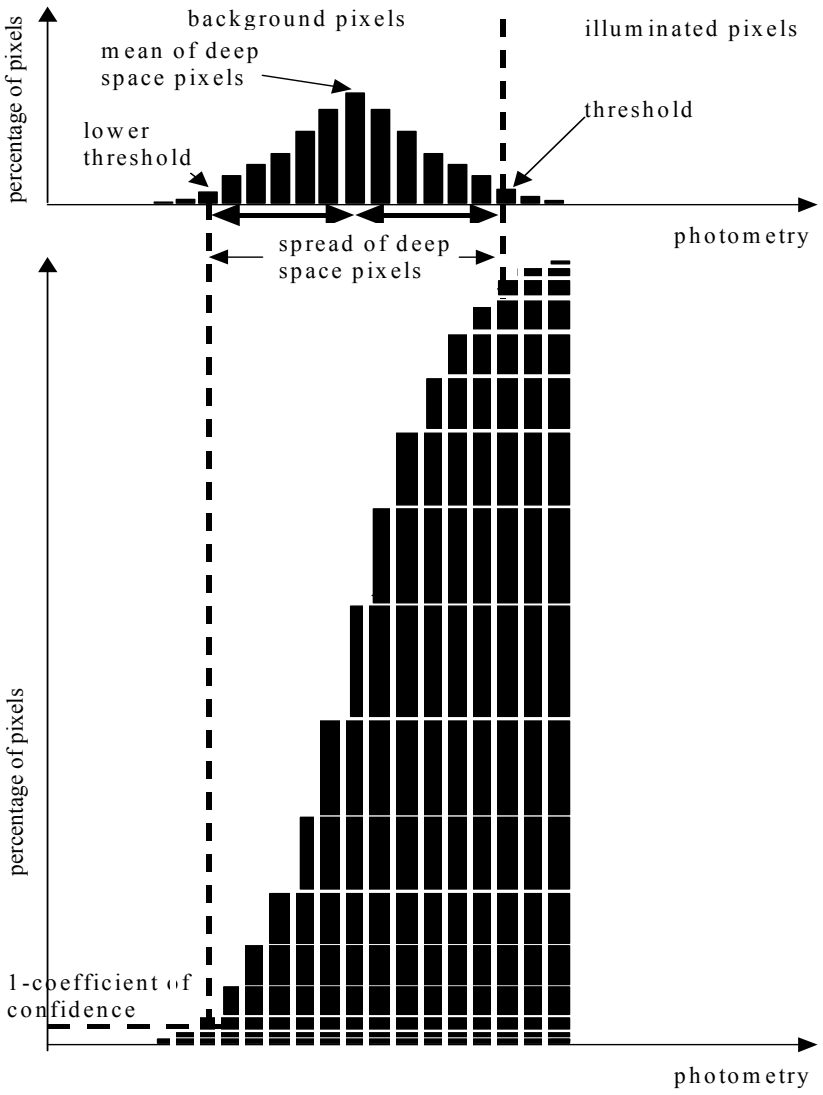

Figure 4 Calculations performed on the image histogram and cumulative histogram

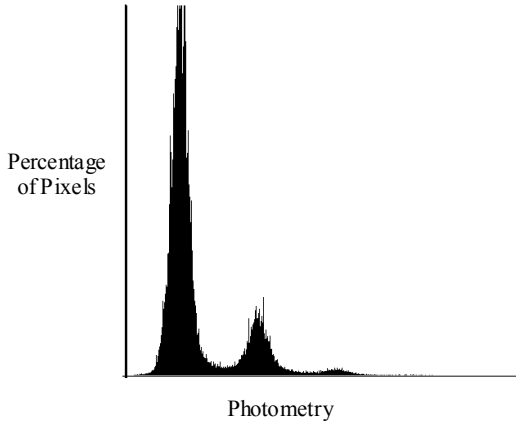

Figure 5 Real image histogram for the image from February 1st 2001. Note that the deep space peak, the star track peak and the satellite cluster peak are all clearly visible, and that all three are approximately symmetrical. Under less ideal image conditions, the peaks are more prone to merging.

Radiometric corrections

Two types of bias are commonly present in a CCD image [4]:

- An additive bias, primarily due to thermal excitation of the CCD array and the resulting drift currents. Removal of this bias results in the subsequent image threshold calculation being less sensitive to CCD array temperature changes.
- A multiplicative bias due to the variation in light sensitivity between the CCD array elements.

The additive bias is suppressed using two reference images:

- an "offset" image taken with the CCD camera shutter closed, with a very short exposure time (of the order of milliseconds), that captures the noise due to the array electronics and any spurious drift currents, and
- a "black" image, also taken with the shutter closed, but for a duration and under conditions similar to those of the real images, to capture the thermal noise.

Taking R as the image to be corrected, O as the offset image and N as the mean black image, the corrected image I is given by:

$$I(x,y) = \big(R(x,y) - O(x,y)\big) - \big(\big(N(x,y) - O(x,y)\big).\rho\big) \qquad (1)$$

where ρ is varied to minimise the influence of dark regions of the image on the thermal noise correction. It is calculated using a sample of deep space pixels.

$$\rho = \frac{\langle R - O \,|\, N - O \rangle}{\langle N - O \,|\, N - O \rangle} \qquad (2)$$

The multiplicative correction is determined using a so-called "flat field" image generated under a bright and uniform sky. Taking R as the image to be corrected (the image after application of the additive correction), F as the flat-field image and K as the mean intensity of the flat-field image, the corrected image I is given by:

$$I(x,y) = K.\frac{R(x,y)}{P(x,y)} \qquad (3)$$

Filtering

In order to improve the subsequent cluster extraction, a simple image filter is applied to smooth the radiometrically corrected image. This involves convolving a 3*3 gaussian mask with the image, the mask *h* defined as

$$h(x,y) = \frac{1}{2\pi\sigma^2}\exp\left(-\frac{x^2+y^2}{\sigma}\right) \text{ with a variance of } \sigma = 1 \qquad (4)$$

This filter replaces each pixel value with a weighted mean of it and its neighbours. The selected filter is symmetric, and can therefore be decomposed into a two-step horizontal and vertical convolution to reduce the computational cost of the filter. Figure 6 shows the previous example image post gaussian filtering.

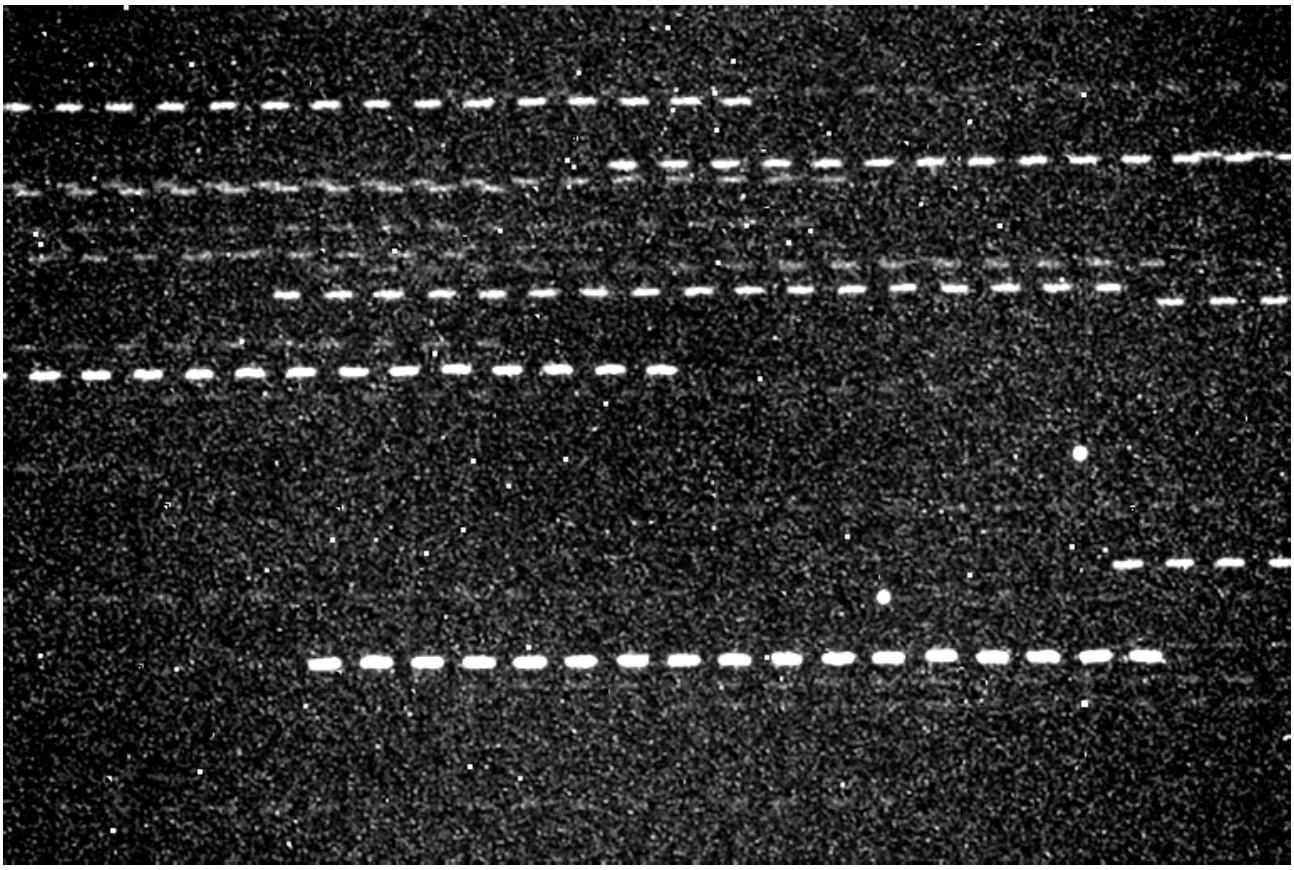

Figure 6 ROSACE image from 1st February 2001 post Gaussian filtering

Extraction of pixel clusters

Having corrected and optimised the image, it is necessary to analyse its content. Initially, the pixel clusters in the image are extracted and classified. The clusters are identified as attached regions of pixels above the image threshold, and their classification results from analysis of their shape.

The entire image is scanned line-by-line, starting in the upper left corner, for pixels with photometric values above the threshold. Upon finding such a pixel, the algorithm searches its neighbourhood recursively for other illuminated pixels.

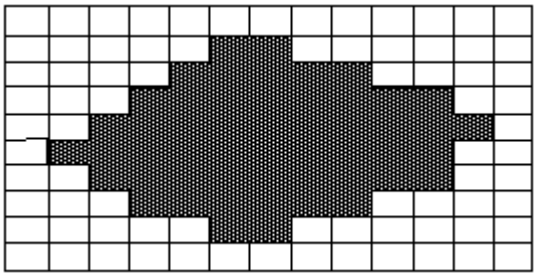

Figure 7 Cluster mask (black represents pixels above the threshold, white below)

Once all neighbouring pixels above the threshold have been found, the cluster is analysed as follows:

- the photometric values for the cluster are recorded.
- a binary rectangular mask surrounding the cluster is generated (as in Figure 7, white representing the pixels within the rectangle that are below the threshold, and black representing those above the threshold, in the cluster).
- a local threshold in the rectangular region around the cluster is then calculated and the binary mask recalculated.
- the barycentre of the cluster is calculated as the geometric centre of the pixels above the threshold, weighted by the photometry of those pixels, as follows:

$$x_b = x_O + \frac{\sum_{cluster} x_i \,\mathrm{Im}(x_i, y_j)}{\sum_{cluster} \mathrm{Im}(x_i, y_j)}, y_b = y_O + \frac{\sum_{cluster} y_j \,\mathrm{Im}(x_i, y_j)}{\sum_{cluster} \mathrm{Im}(x_i, y_j)} \quad \textbf{(5)}$$

where
(x_b, y_b) are the coordinates of the barycentre,
(x_O, y_O) are the coordinates of the origin of the mask,
(i, j) are the points in the cluster mask and
Im is the matrix of image pixels

- the form of the cluster is analysed to determine whether it is elongated (as in star clusters), circular (as in satellite clusters) or potentially anomalous, using the inertia matrix of the cluster mask region, I, as follows:

$$I = \begin{bmatrix} I_{xx} & I_{xy} \\ I_{xy} & I_{yy} \end{bmatrix} \quad \textbf{(6)}$$

where

$$I_{xx} = \sum_{cluster} (y - y_b)^2 \,\mathrm{Im}(x, y),$$

$$I_{xy} = \sum_{cluster} (x - x_b)(y - y_b) \,\mathrm{Im}(x, y) \text{ and}$$

$$I_{yy} = \sum_{cluster} (x - x_b)^2 \, \mathrm{Im}(x, y),$$

(x_b, y_b)	are the coordinates of the barycentre,
(x, y)	are the points in the cluster mask and
Im	is the matrix of image pixels

from which the elongation *e* of the cluster is calculated as:

$$e = \begin{cases} \sqrt{\dfrac{I_{\max}}{I_{\min}}} & I_{\min} \neq 0 \\ 0 \quad otherwise \end{cases} \qquad (7)$$

Values of *e* close to 1 identify the cluster as circular and those greater than a specifiable threshold are identified as elongated.

Clusters that contain too few pixels, pixels that are saturated, or that are too close to other clusters, and those with neither a circular nor elongated form, are eliminated from further investigation. Once this cluster analysis has been completed, the pixels concerned are deleted from the filtered image and the cluster search continues.

Alignment detection

The alignment detection applies a Hough transform to the valid cluster barycentres in the image, to find the possible alignment directions within the image. The Hough transform uses a particular parameterisation of lines, namely the angle α measured with respect to one of the image axes and the perpendicular distance d between the line and the centre of the image, as illustrated in Figure 8.

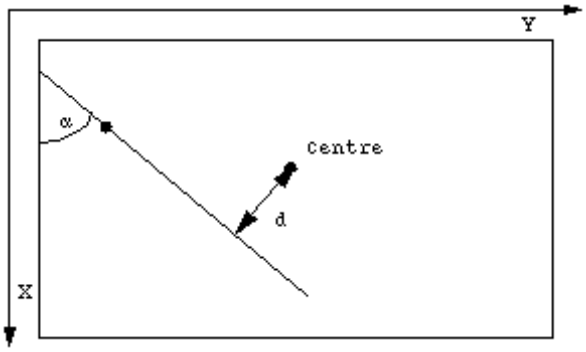

Figure 8 Parameters for the Hough Transform

Defining the line space thus allows it to be discretised by angle and distance. The Hough matrix dimensions are then defined as having the same number of rows as discrete angle ranges selected, and the same number of columns as the discrete distances selected. Having defined the size of angle and distance bins, each barycentre in the image can be analysed. For each mean bin angle in the Hough matrix, the corresponding distance to the centre of the image for a line passing through the barycentre in question is calculated, and the corresponding angle-distance bin in the Hough matrix is incremented. Once all the barycentres have been analysed, only the bins in the matrix with sufficient points are kept, which represent the best starting lines from which to find complete star tracks in the image.

To improve the star track directions, a subsequent classic regression analysis is applied: for each line extracted from the Hough matrix, the perpendicular distance to each barycentre is calculated, and the barycentres within a few pixels of the line are identified as associated with that line. The new star track directions are then defined by the classic regression lines passing through the identified barycentres.

Having obtained the new star tracks, the list of barycentres is reassessed to ensure association only between the new line and those centres within the specified distance of the line.

The resulting alignments and associated barycentres are then subjected to a number of quality controls to remove spurious cases, to result in the final set of star tracks. The spurious cases include incomplete star tracks where the number of barycentres associated with a track is less than the number of shutter cycles in the image, and double tracks where two tracks have the same alignment in the image (identified by comparing the photometries of clusters associated with the line, and by ensuring the barycentres of the clusters are not separated by more than a specified distance). The mean of the barycentres associated with each star track is then taken as the track barycentre. Finally, the track and satellite barycentres are assigned a timestamp based on the mean of the shutter times recorded with the image.

Identification

Having analysed the star tracks and satellite cluster(s) and calculated their barycentres, the stars and satellite(s) must be identified using a catalogue of stars and satellites in order to determine their angular positions precisely.

The satellite catalogue contains the orbital bulletins for each of the observed satellites, provided during the planning phase of the campaign. These orbital bulletins must be sufficiently precise in the case of collocated satellites to be able to distinguish between the satellites in the image. For single satellites however, the orbits can be less precise: the satellite cluster closest to the predicted satellite location is taken to be the correct match, with a large tolerance on the distance between predicted and actual locations.

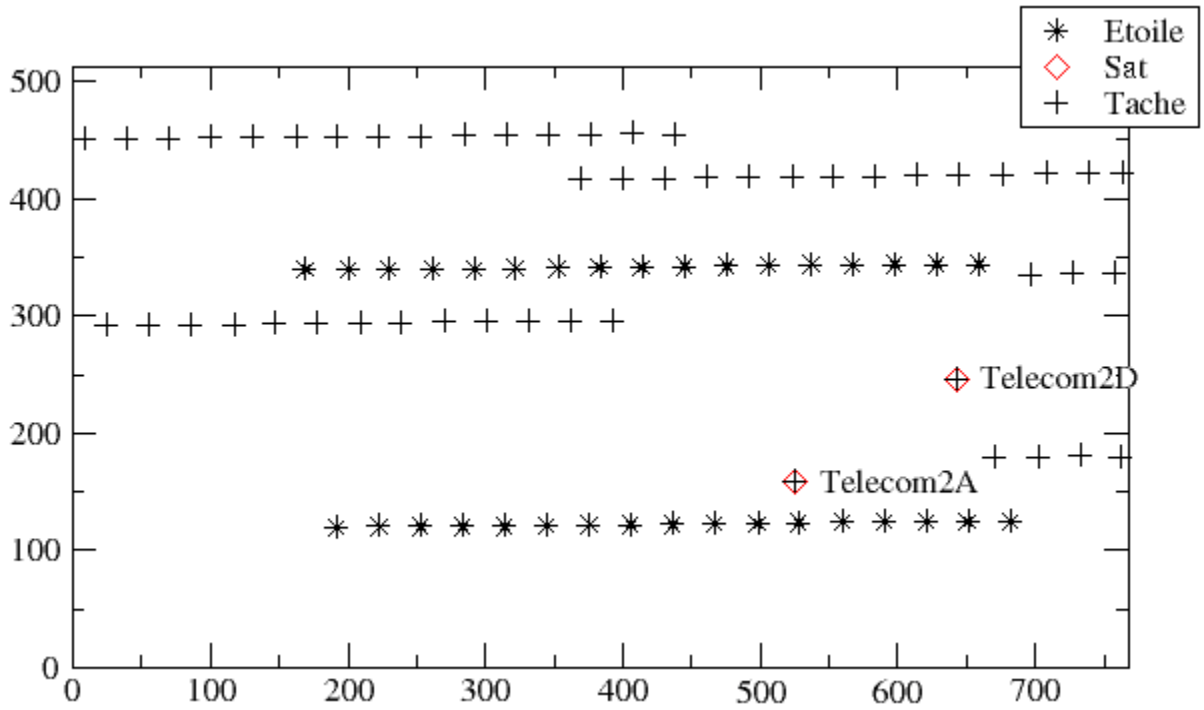

Figure 9 Identified satellites and stars for the image of February 1st 2001

The star catalogue used has been extracted from the Tycho star catalogue created as part of ESA's Hipparcos mission. The ROSACE star catalogue has retained from its larger relation the star ID, equatorial coordinates (right ascension and declination) on J1991,25 in the ICRF reference frame, coordinate error magnitudes in the same reference frame, the star magnitude, the motion characteristics by

julian date and the error magnitudes in the motion characteristics. From this, the position of each star is determined in terms of azimuth and elevation from the station at the time of each image.

Identifying the stars in the image is then achieved by transforming the position of the star track barycentres in image coordinates to azimuth and elevation relative to the station. These are then matched with the values for the stars in the catalogue. Figure 9 shows the pixel clusters found in the image from February 1st and the resultant identified stars and satellites. As at present the alignment analysis requires complete star tracks to have been identified, it can be seen that all complete star tracks and both satellites have been identified for this image.

Measurements

The basic measurement from the image is an angular distance measurement. The two angles η and φ between the barycentre of each satellite and each star track in turn (see also Figure 1) are converted to azimuth and elevation relative to the station using the precise location of the stars given in the star catalogue, and various conversions between frames of reference and rotations, as shown in Figure 10.

The star catalogue allows the precise star position D and station-star direction $\vec{u}_D$ to be determined. The satellite (F) can then be said to be sat on the cone of axis (S, $\vec{u}_D$) and of half-angle η. The intersection of the star track with this cone (point D') is then given by the rotation of the telescope mount by $\vec{\omega}_{M/i}$ in the inertial frame.

The station-satellite direction $\vec{u}_F$ is then described by the direction station-D' rotated about the axis $\vec{u}_D$ by the angle φ. This direction vector is then simply converted to azimuth and elevation from the station. The elevation measurement is then finally corrected for tropospheric effects.

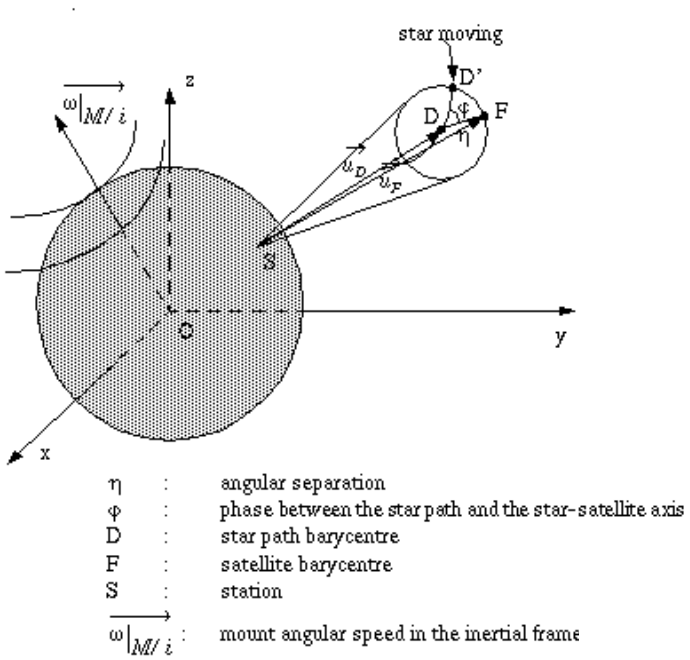

Figure 10 Calculation of the station-satellite direction from the ROSACE angle measurements

RESULTS & CONCLUSIONS

After installation of the first ROSACE station at OHP at the start of 2001, it was proposed to run measurement campaigns on geostationary satellites to evaluate the precision of the ROSACE measurements. No direct external calibration system was available, therefore the validation was performed using orbits restituted from the measurements for the satellites followed during the campaign. Orbit restitution using the measurements from a single ROSACE station require a relatively long period of observation, at least two consecutive nights of measurements to provide good coverage of the satellite through the complete geostationary arc. It was therefore necessary for validation to perform campaigns over a number of days, to allow useful analysis of the coherence of the reconstituted orbits with the measurements taken over disjointed parts of the geostationary arc.

A certain number of technical difficulties with the prototype station, coupled with particularly poor meteorological conditions over the past year, resulted in fewer validation campaigns than had been hoped. The station has in contrast been used to generate a number of measurements over relatively short observation periods, of little use for orbit restitution, but rich in information regarding the performance of the system as a whole. In particular, the limitations of the image collection and processing were able to be assessed during the summer months. The image quality was found to be degraded during the summer, highlighting an additional constraint to the site requirement on numbers of clear nights, as this does not in itself guarantee good quality images from the point of view of astronomy. In particular, atmospheric turbulence induced by hot weather results in somewhat 'milky' and poorly contrasted images. The performance of the image processing algorithms on these poorer images was also found to be degraded, resulting in a number of potential improvements being identified, which are discussed after these results in the proposed future work.

The results presented here consist of the measurements taken over the five consecutive nights from January 29th to February 3rd of the satellites Telecom2A and Telecom2D (T2A and T2D respectively), collocated at –8 degrees, and Telecom2C (T2C) at –5 degrees. For each satellite, approximately 250 measurements of azimuth and elevation were obtained over the five nights, and these were used to restitute the orbits.

The orbit restitution software is based on the method of least squares, whereby the parameter estimation consists of minimising the residuals (between the measurements and their ideal equivalents resulting from the estimated orbit) globally over the period analysed [5]. The estimated parameters are the six orbit parameters and the multiplicative constant of solar radiation pressure, K.

The period of restitution was varied to analyse the measurement residuals for each set of data, and to determine the coherence of the restituted orbits over the different measurement angles. For T2D, the radial, tangential and normal components of the two stationkeeping manœuvres executed during the campaign (on 30/01/2001 at 22H22 and on 01/02/2001 at 18H15) were also determined.

The results are given in Table 1 below, showing for each set, the satellite concerned, the parameters that were estimated, the number of nights of measurement used in the calculation and the mean values and RMS residuals in azimuth and elevation. The order of magnitude of the residuals and the nature of their spread provide a good indication of the quality of the orbit.

From the table below, it is clear that however the orbit reconstitution was performed, the residuals for both axes were both coherent and relatively small: an RMS value of approximately $0.17*10^{-3}$ degrees in elevation, and $0.25*10^{-3}$ degrees in azimuth, with means of approximately zero.

Table 1 T2A and T2D orbit restitution and residuals

Satellite	Estimated parameters	Number of nights	Elevation Residuals		Azimuth Residuals	
			Mean (deg)	RMS (deg)	Mean (deg)	RMS (deg)
T2A	Orb + K	5	$-0.5\ 10^{-5}$	$0.165\ 10^{-3}$	$0.9\ 10^{-6}$	$0.247\ 10^{-3}$
T2A	Orb + K	4	$-0.7\ 10^{-5}$	$0.165\ 10^{-3}$	$0.1\ 10^{-5}$	$0.249\ 10^{-3}$
T2A	Orb + K	3	$-0.8\ 10^{-5}$	$0.165\ 10^{-3}$	$0.9\ 10^{-6}$	$0.233\ 10^{-3}$
T2A	Orb	2	$-0.1\ 10^{-4}$	$0.168\ 10^{-3}$	$0.2\ 10^{-5}$	$0.229\ 10^{-3}$
T2C	Orb + K	5	$-0.6\ 10^{-5}$	$0.166\ 10^{-3}$	$-0.9\ 10^{-6}$	$0.235\ 10^{-3}$
T2C	Orb + K	4	$-0.6\ 10^{-5}$	$0.164\ 10^{-3}$	$0.1\ 10^{-5}$	$0.228\ 10^{-3}$
T2C	Orb + K	3	$-0.3\ 10^{-5}$	$0.165\ 10^{-3}$	$0.4\ 10^{-6}$	$0.236\ 10^{-3}$
T2C	Orb	2	$-0.5\ 10^{-5}$	$0.173\ 10^{-3}$	$0.9\ 10^{-6}$	$0.261\ 10^{-3}$
T2D	Orb + ΔV1 + ΔV2	5	$-0.8\ 10^{-5}$	$0.166\ 10^{-3}$	$0.2\ 10^{-5}$	$0.218\ 10^{-3}$

The order of magnitude of the smallest eigenvalue from the least squares calculation provides an indication of the *observability* of the estimated parameters, where too small a value indicates a lack thereof. It was apparent from the results that at least three nights of measurements were required to estimate correctly the coefficient of solar radiation pressure: with only two nights of measurements, the value of the coefficient was not at all realistic: 1.82 where it should be of the order of 1.0, and the smallest eigenvalue was $3*10^{-5}$ (whereas with 5 nights of measurements, it achieved the more reasonable value of 10^{-3}). It is worth noting however that the periods of measurement for the nights concerned were relatively short, and it may be that two longer nights of measurement would suffice.

The coefficient K was also not able to be calculated at the same time as the 6 orbital parameters and the 3 components of each manœuvre in the case of T2D: the measurements were not able to provide sufficient information to make a reliable estimation of as many parameters. To estimate all the parameters, measurements more spread out across the manœuvres would be necessary.

Whilst it may seem that the observation period required to estimate all the parameters is relatively long, it is worth reiterating that the results presented were for a single station, that only provides angular data. Adding a second station ideally separated by a relatively large distance would increase the observability and hence reduce the number of nights necessary for estimating all the parameters reliably.

The plot of residuals over time is provided in Figure 11. This provides useful additional information to the mean residuals themselves as it shows up any periodic effects or slope in the values of the residuals with time, which may be masked by the overall mean and RMS values.

Again it is clear from the plots that the residuals for T2A and T2D over the five days of measurement are well centred about 0 for the whole campaign. Given the length of arc analysed (5 days), the restituted orbit can be said to be coherent with the measurements over an extrapolation of 5 days. The plots of residuals for T2C was similar.

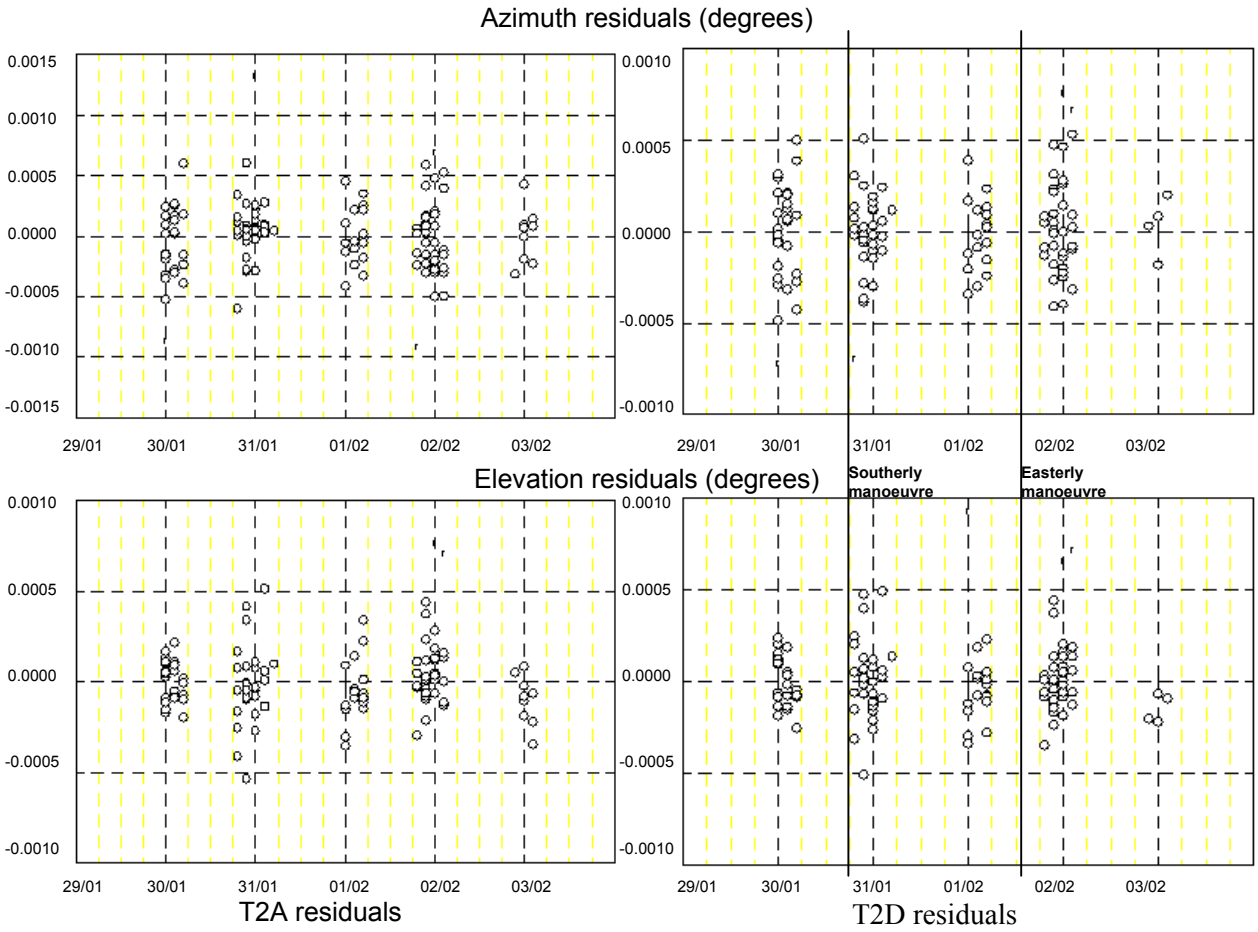

Figure 11 Plot of residuals for the T2A and T2D reconstituted orbits, in azimuth and elevation

The stability of the orbit alignment can equally be analysed by comparing orbits restituted on measurements taken over overlapping parts of the geostationary arc. The discontinuity in satellite position during the overlapping period for the two orbits generated gives an idea of the position precision.

The T2A orbit was reconsituted over the first three days of measurement and the last three days, resulting in an overlap of one night's measurements.

Table 2 and Figure 12 present the results of the two orbit comparison for the 1st of February, in terms of the separation between the resulting satellite positions in radial, tangential and normal directions.

Table 2 Orbit alignment stability

Gap	Mean separation (m)	Standard deviation (m)
radial	4.8	15,0
tangential	0,1	38,9
normal	-39,5	23,9

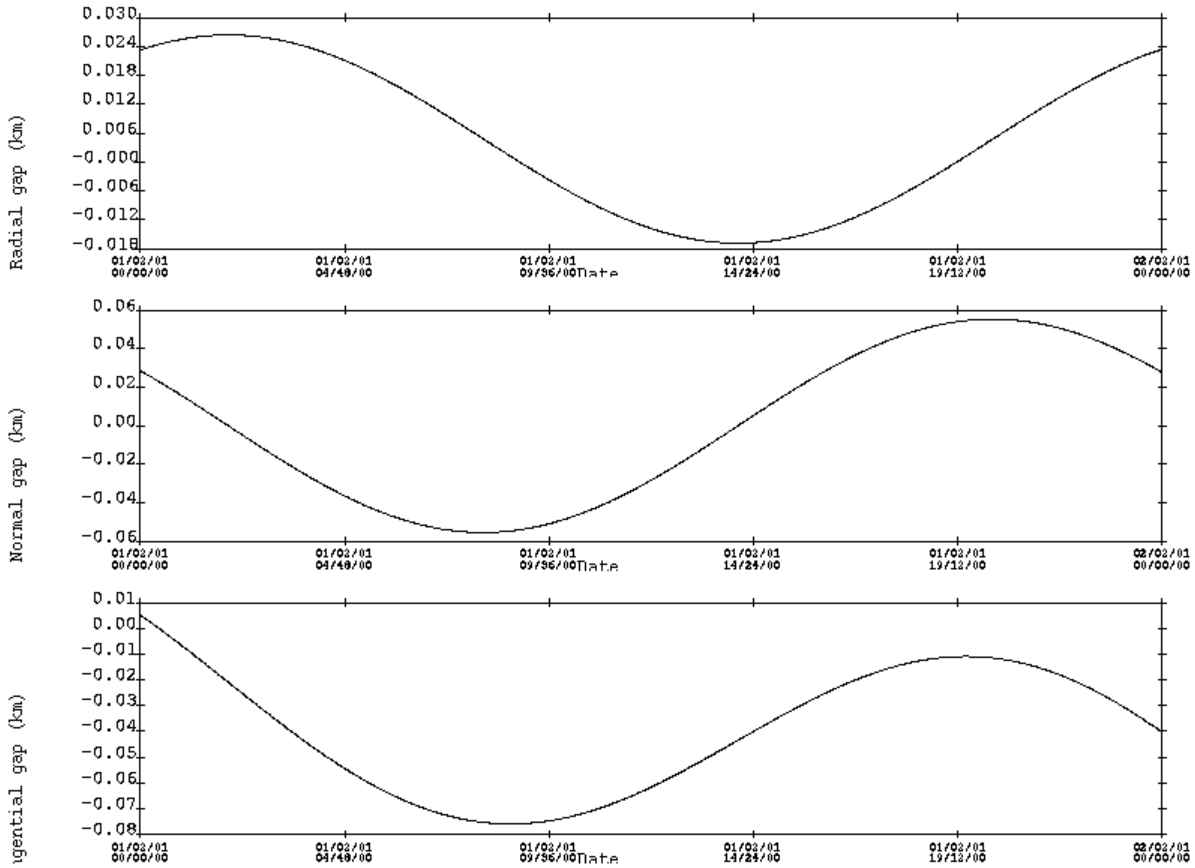

Figure 12 Differences in satellite position for the T2A orbits reconstituted with only the first 3 and last 3 days of measurements

Over the 24h period of comparison, the separations are of the order of some tens of metres, with a periodic effect. The orbits restituted are therefore coherent to the degree of precision given by the earlier residuals.

For T2D, the estimated manœuvres were also compared to those calculated by the Telecom satellite control centre, using its turn-around based measurements. Table 3 presents the radial, tangential and normal components of the southerly manœuvre from February 20th and the easterly manœuvre from the 1st of February.

Table 3 Estimation of the first T2D manoeuvre from January 20th

Estimated DV (m/s)	Turn Around	ROSACE
DVR_1	-0.114	-0.109
DVT_1	-0.083	-0.082
DVN_1	-2.281	-2.288
DVR_2	+0.042	+0.046
DVT_2	+0.086	+0.086
DVN_2	-0.016	-0.011

The differences can be seen to be relatively small, of the order of some mm/s, showing that the ROSACE manoeuvres are indeed very close to those obtained by the control centre's turn-around system using two stations well separated.

These results alone, which only cover measurements over a few days, are insufficient to validate any statement on the precision on ROSACE measurements. They do however show that the measurements are of good quality, the residuals at 1σ being of the order of 0.6 arcseconds in elevation and 0.9 arcseconds in azimuth. This does not quite achieve the hoped precision of 1 arcsecond at 3 σ, but they are nonetheless very good first results.

The prototype station has therefore proven the ROSACE concept and has shown to be able to provide satellite position measurements suitable for orbit determination. Whilst the hoped precision has not been obtained from the first results, the station has already been shown to be much more precise than the standard localisation systems using ranging, typically able to provide precision no better than 10^{-2} degrees (i.e. 30-40 arcseconds). Combined with the low cost of the station, this provides an encouraging basis for future operational use of ROSACE stations. It is hoped to develop further stations in the near future, both to improve the availability of the system, to obtain better results from combining multiple measurements and to benefit from better conditions for astronomical observation available overseas.

FUTURE WORK

The ideal for calibrating a satellite localisation system is to use another system of greater or equal precision, and determine the residuals of the measurements from the system to be calibrated with the orbits reconstituted from the reference system. The upcoming STENTOR mission has been targeted to achieve this type of calibration: STENTOR will make use of very precise active ground localisation systems (so-called SLF stations, based on GPS pseudolite signals [6]), for validation of its ion thruster performance. These will provide localisation of the order of a few metres in each axis. ROSACE is in fact one of the experiments associated with STENTOR, as it is intended to use the ROSACE station to assist with day-to-day stationkeeping activities after the initial thruster calibration using the SLF stations, to improve upon the precision of the subsequently available standard ground localisation systems.

Equally, as this is a different type of measurement from those provided by existing localisation systems, it is necessary to study its characteristics and its optimal use when coupled to other measurement types: in effect, distance measurement localisation systems do not provide the same input to the orbit determination calculations as angular measurements. Just as distances give a better observability of an orbit's semi-major axis, so angular measurements provide better angular parameter estimates. Knowing how and when best to combine data, and whether traditional localisation data collection cycles can be reduced by suitable combination of ROSACE measurements is therefore one of the next goals for the project.

To assist in this aim, a concerted effort is being made to perform joint measurement campaigns between existing ground stations and ROSACE for analysis of the comparative orbits.

As regards the image collection and processing, to date the images collected have been reduced using 2*2 pixel binning. It is intended to move to the full resolution, resulting in images of 1024*1536 pixels, in the near future. This will allow the cluster barycentres to be calculated more precisely, resulting in a consequent precision increase in the measurements themselves.

Following the collection of images under less than ideal observation conditions, in particular during the summer months, a number of evolutions in the image processing are also currently in progress. These aim both to increase the number of measurements obtainable from poorer quality images (thus effectively increasing station availability) and to improve the precision of cluster barycentre calculation in all images, (consequently improving measurement precision) by using more of the prior knowledge regarding the images *earlier* in the image processing cycle. For example, using the number and length of shutter cycles, and the likely star directions from the star catalogue for the given telescope pointing, it is possible to

produce a reference image, which can subsequently be matched globally with the real image to provide the measurement angles directly.

On development of further ROSACE stations, another area of analysis to be investigated is that of optimal combination of station measurements and planning of coordinated campaigns.

REFERENCES

[1] L. Maisonbe, B. Lazard, “ROSACE Autonomous orbit determination system using deviation on CCD”, *IAF Conference*, Graz, Austria, October 1993.

[2] E. Cazala-Hourcade, P. Tayrac, “Constitution d’une mesure rosace, restitution d’orbite par système autonome CCD d’écartométrie”, *Spaceflight Dynamics*, Toulouse, France, June 1995.

[3] C. Buil, A. Klotz, E. Thouvenot, “QMIPS32 Image Processing Software”, *http://www.astrosurf.com/re/qmips32.html*

[4] C. Buil, E. Davoast, “CCD Astronomy: Construction and use of an astronomical CCD camera”, *Willmann-Bell*, January 1991.

[5] J-P. Carrou, “Mécanique Spatiale Tome I”, *Cépaduès-Editions*, 1995.

[6] J. Barbier, F. Saffre, "High performance low cost ranging system for STENTOR GEO payload", *ION-GPS*, Salt Lake City, 2000.